Carbohydrate Polymers 190 (2018) 262–270

Contents lists available at ScienceDirect

Carbohydrate Polymers

journal homepage: www.elsevier.com/locate/carbpol

New cellulose crystallinity estimation method that differentiates between organized and crystalline phases

Umesh P. Agarwal*, Sally A. Ralph, Richard S. Reiner, Carlos Baez

Fiber and Chemical Sciences Research, USDA FS, Forest Products Laboratory, 1 Gifford Pinchot Drive, Madison, WI, 53726-2398, United States

ARTICLE INFO

Keywords:
Cellulose crystallinity
Raman spectroscopy
Low frequency
Organized
Crystalline
Hydrothermal
Wood

ABSTRACT

A new method is proposed for estimation of cellulose crystallinity (CrI) based on 93 cm^{-1} Raman band in spectra of cellulose I materials. In this method (93-Raman), CrI was determined based on regression that was developed using the ratios of peak-heights of the 93 and 1096 cm^{-1} Raman bands (I_{93}/I_{1096}). For calibration purposes, a set of eight samples, all derived from cotton microcrystalline cellulose Whatman CC31 were selected. When the peak intensity ratios (I_{93}/I_{1096}) were plotted against the calculated CrIs of the calibration set samples, the plot showed an excellent linear correlation ($R^2 = 0.9888$). The 93-Raman method was used to estimate crystallinities of a number of cellulose materials including poplar wood samples that were hydrothermally treated at various temperatures. The wood 93-Raman CrI data showed that the method is able to differentiate between organized and crystalline phases of cellulose, a capability lacking in many other CrI estimation methods.

1. Introduction

Cellulose crystallinity (CrI) is one of the most useful characteristics of renewable and biodegradable materials because it plays an important role in their physical, mechanical, and chemical properties. In such materials, the final state of cellulose aggregation depends upon the processing and treatment conditions used, e.g., temperature, pressure and specific treatments (mechanical, chemical, and biological) involved. In order for a particular cellulose supramolecular state to qualify as crystalline, the solid state structure has to fulfill the requirements of (a) spatial order and (b) long range translational symmetry (that way, repetition of the unit cell generates the entire superstructure). Presence of condition (a) in itself is not sufficient (Bower and Maddams, 1989). Although controversial, it has been reported that while in the native state wood cellulose is spatially ordered, it was found to be non-crystalline (Agarwal, Ralph, Reiner, & Baez, 2016). This suggests that the native aggregated state of wood cellulose lacks long range translational symmetry. Moreover, recent findings have suggested that the presence of the spatially ordered cellulose (e.g., a mono layer thick lamella of cellulose chains) is likely to influence the estimates of CrI by the NMR, XRD, and Raman methods (Li and Renneckar, 2011; Li, Sathitsuksanoh, Zhang, Goodell, & Renneckar, 2017; Su, Burger, Ma, Chu, & Hsiao, 2015). This is due to the fact that in these methods, non-crystalline ultrathin microfibril fractions that are only molecularly thick (0.5 nm) and contained only a single layer of cellulose chains contributed in the same regions where contributions of crystalline domains are detected (Li and Renneckar, 2011; Li et al., 2017; Su et al., 2015). Therefore, such assemblies of cellulose which are clearly non-crystalline, when present, will contribute towards the estimated CrI of a material. On the other hand, a similar limitation was encountered for the 380-Raman method when it was used to calculate the CrI of native wood celluloses. For instance, the method produced CrI values of 49.9 and 57.4% for aspen and red pine woods, respectively, although no crystalline cellulose domains existed in these woods (Agarwal et al., 2016; Agarwal, Reiner, & Ralph, 2013). This further supported the argument that cellulose that is simply ordered spatially and not crystalline is capable of making contributions in the spectral/diffraction regions that are typically associated with crystalline cellulose. Further, in XRD, wood and other low CrI celluloses showed high sensitivity to moisture induced changes – depending upon the samples, the crystallinity increased by as much as 40% (Agarwal, Ralph, Baez, Reiner, & Verrill, 2017), such evidence supported the existence of spatially organized but non-crystalline cellulose. In the context of cellulose, by spatially organized, the structure is meant to be composed of aligned (in the same direction) molecules that interact via H-bonds in many ways.

Therefore, in view of the limitations of the existing approaches to estimate cellulose CrI, a new method is needed. Here, a new approach

Abbreviations: XRD, X ray diffraction; NMR, nuclear magnetic resonance; SEM, scanning electron microscopy or scanning electron micrograph; FT, Fourier-transform; IR, infrared; LF, low frequency; MCC, microcrystalline cellulose; WAXS, wide angle X-ray diffraction; CrI, crystallinity; RO, reverse osmosis; CNCs, cellulose nanocrystals; PH, peak height

* Corresponding author.
E-mail address: uagarwal@fs.fed.us (U.P. Agarwal).

https://doi.org/10.1016/j.carbpol.2018.03.003
Received 5 December 2017; Received in revised form 27 February 2018; Accepted 2 March 2018
Available online 05 March 2018
0144-8617/ Published by Elsevier Ltd.

Table 1
Percent Crystallinities of calibration set samples—calculated, Segal-WAXS, 380-Raman, and 93-Raman.

Sample ID	Mass ratio control:120 min ball-milled, grams	Calculated[a]	Segal-WAXS[b]	380-Raman[c]	93-Raman[d]
Control	0.5000:0.0000	80.5	80.5	78	74.7 ± 0.92
Mixture 1	0.4030:0.1042	64.0	56.7	62.7	63.4 ± 0.70
Mixture 2	0.3232:0.1800	51.4	53.4	52.8	52.9 ± 0.49
Mixture 3	0.2733:0.2188	44.8	47.0	44.8	46.3 ± 1.79
Mixture 4	0.2053:0.2963	33.0	42.6	36.2	35.7 ± 0.90
Mixture 5	0.1299:0.3722	20.9	26.7	23.1	21.8 ± 0.29
Mixture 6	0.0675:0.4331	10.9	17.4	11.3	9.6 ± 1.64
120 min ball-milled	0.0000:0.5000	0.0	−1.0	−4.4	−3.7 ± 0.18

[a] Except for control and 120-min milled which were WAXS crystallinities (for 120 min ball milled sample, −1% was taken as 0%).
[b] Calculated according to Agarwal et al. (2010).
[c] Estimated according to Agarwal et al. (2010, 2013).
[d] Based on the peak height method.

based on low frequency Raman spectroscopy is proposed. Prior to 1995, Raman spectra of celluloses were obtained using systems that were visible laser based and were not capable of detecting bands in the frequency region below 200 cm^{-1}. This was due to a strong contribution from Rayleigh scattering which masked weak low frequency (LF) Raman scattering from samples. The optical components typically used in filter based Raman spectrographs could not effectively reject the Rayleigh signal. In the mid 1990s, after the 1064 nm based spectrometers became commercially available, LF spectra could be obtained. However, to the best of our knowledge, it was not until 2014 that the first low frequency (< 200 cm^{-1}) Raman spectra of cellulose materials were published (Agarwal, 2014). The primary author has previously reported the existence of a 93 cm^{-1} Raman band, in the spectra of highly crystalline cellulose (Agarwal et al., 2016; Agarwal, 2014). Moreover, it was reported that the 93 cm^{-1} band intensity declined for lower CrI materials and disappeared completely in the Raman spectrum of amorphous cellulose. Further, for materials composed of cellulose II and cellulose III polymorphs, either the band was missing or significantly weaker (Agarwal, 2014). Most importantly, hardly any intensity at the 93 cm^{-1} band was observed for a NaOH treated wood holopulp sample air dried at 25 °C (Agarwal et al., 2016). It's important to note that in the holopulp sample most lignin and hemicellulose was removed (Agarwal et al., 2016). This indicated that spatially ordered but non-crystalline cellulose did not contribute to the band at 93 cm^{-1}.

The LF Raman spectroscopy (< 200 cm^{-1}) probes the same low energy vibrational and rotational modes of materials as terahertz spectroscopy (300 GHz–6 THz) (Parrott and Zeitler, 2015). The latter technique has been used by Vieira and Pasquini (Vieira and Pasquini, 2014) to study microcrystalline cellulose and a band at 3 THz (corresponds to 99.9 cm^{-1}) was detected. Subsequently, the researchers used this band to develop a terahertz-time domain spectroscopy method for determination of cellulose CrI. The LF Raman and terahertz time domain spectroscopy have been used in numerous studies of organic molecular crystals because low photon energy makes it possible to excite intermolecular motions (Parrott and Zeitler, 2015).

The objective of the present investigation was to develop a new method for estimating CrI of cellulose that is capable of distinguishing between organized/ordered and crystalline celluloses. Such a method will be highly useful to the researchers working in the field of cellulose science because the CrI data will be free of contributions of non-crystalline organized cellulose. In the present study, the authors have used the intensity of the 93 cm^{-1} Raman band to accomplish this goal. The principle behind the present Raman methodology is that the intensity of the 93 cm^{-1} spectral feature is affected by cellulose CrI. Moreover, it is known that in vibrational spectroscopy, only two kinds of vibrational modes are detected in the low frequency region − hydrogen-bonds and crystal modes (Parrott and Zeitler, 2015; Paolantoni, Sassi, Morresi, & Santini, 2007). Contributions from the former were ruled out based on the fact that no shift in the position of the 93 cm^{-1} band was observed in the deuterated crystalline samples of cellulose (more later). Therefore, the band at 93 cm^{-1} in the spectra of cellulose materials is likely to represent one of the lattice modes of crystalline cellulose. Once the 93-Raman method was developed for estimating CrI, it was applied to a variety of cellulose containing materials that included woods, pulps, microcrystalline celluloses, tunicin, and cellulose nanomaterials.

2. Experimental

2.1. Chemicals

Unless stated otherwise, all chemicals and reagents were purchased from Sigma–Aldrich (St. Louis, MO).

2.2. Celluloses

Avicel pH −101 was obtained from FMC Corporation (American Viscose Division, Newark, Delaware). Cotton microcrystalline cellulose (MCC) Whatman CC31 powder was from Whatman International Ltd., (Maidstone, UK). Amorphous cellulose sample was generated by grinding, for 120 min, Whatman CC31 in a vibratory mill using steel balls. The milling was conducted in a cold room (5 °C). For calibration purposes, cellulose mixtures with crystallinities in the range 10.9–64% were produced using different mass fractions of 80.5% crystalline cellulose I Whatman CC31 and completely amorphous cellulose (120 min ball-milled Whatman CC31). This group of six samples (mixtures 1–6, Table 1) along with the control and 120 min milled Whatman CC31 were used as calibration set for the present study. The same samples have been used previously in the development of the 380-Raman CrI method (Agarwal, Reiner, & Ralph, 2010).

Tunicin was isolated from tunicates which were provided by Dr. Johan Foster (Virginia Tech). The tunicin isolation procedure was as follows. A frozen tunicate specimen was thawed and split. A portion was taken from the "knobby" orange top (tunic), the tan "wrinkled" bottom and the fibrous "root" sections. Raman sampling of these three portions indicated that the tunic portion had the highest cellulose content. The tunic portions of the tunicates were removed. A 4 l glass beaker containing 1.5 liters of RO water and a stir bar was heated to 80 °C and 75 g of sodium hydroxide was added and dissolved. The frozen tunicate pieces were added and left to stir at that temperature for 6 h. The solution appeared yellow/orange and the tunicate was less colored. The base solution was decanted and the tunicates were washed with several exchanges of RO water. The material was added to 1500 ml of RO water, 75 g of sodium hydroxide was added and the solution brought up to 60 °C with stirring. The heat was turned off but the stirring was continued overnight. The following morning the sample was again heated to 80 °C and left to stir for 8 h. The solution was only faintly yellow. The solution was then decanted and the material washed copiously with RO water. 1500 ml of RO water was then added along

with 3.5 ml of Clorox bleach (6% sodium hypochlorite) and 2.5 ml of acetic acid. The heating (80 °C) and stirring were continued for 1 h. An additional charge of the bleach and acid was added and this was repeated 60 min later. The sample was left to stir overnight without heat. The following morning, the sample was decanted and stirred with RO water and washing was done eight times. The sample was then drained, bagged, and frozen.

2.3. Pulp, woods, and hydrothermally treated woods

Softwood bleached kraft pulp and aspen and poplar woods were available in our laboratory and had been obtained previously in the context of other projects. The woods were Wiley milled to 40 mesh and extracted with acetone:water (9:1). For hydrothermal treatment at 200 °C in H_2O and D_2O, 5 g of air-dried, 40 mesh Poplar (95% solids) was added to 40 ml of water (or D_2O). The above was placed in a Teflon-lined Berghof reactor vessel that was sealed, brought to 200 °C over a 75 min ramp and held at temperature for 90 min. The reaction was quenched by placing the vessel in a cold-water bath. The treated wood and solution were filtered through a sintered glass funnel and were washed with RO water (H_2O) until the filtrate was almost colorless. A portion of the filter-cake was treated at 70 °C over 9 h with 5 treatments of sodium chlorite and acetic acid as per the method of Ahlgren and Goring (Ahlgren and Goring, 1971). The residual, delignified treated wood was thoroughly washed with RO water but had some residual color and again was stored as the wet filter-cake. The delignified wood (holopulp) was further treated with 4% NaOH at 70 °C for 4 h to remove any residual lignin and some of the present hemicelluloses. This alkali treated sample was used for Raman analysis. Similarly, additional hydrothermal treatments of poplar were also carried out at 135 and 170 °C. These two samples along with the portion of control poplar wood were subjected to similar delignification and alkali treatments. Additionally, portions of milled aspen wood were bleached with alkaline H_2O_2 and acid chlorite delignified according to the methods previously reported (Agarwal et al., 2013).

2.4. Cellulose nano-crystals (CNCs) production from bleached kraft pulp and hydrothermally treated wood

Pulp CNCs were produced from bleached softwood kraft pulp using the previously reported method (Agarwal et al., 2016; Reiner and Rudie, 2013). The process uses 64% sulfuric acid at 45 °C. Further details of the process can be found elsewhere (Agarwal et al., 2016; Reiner and Rudie, 2013).

2.5. SEM imaging

Control Whatman CC31 and 120 min ball-milled Whatman CC31 samples were examined and photographed with a Zeiss EVO 40 SEM (Carl Zeiss SMT Inc., Thornwood, NY). The particles were dispersed in water and air dried. The samples were sputter-coated with gold using a Denton Desk-1 sputter coater (Cherry Hill, NJ) to provide sufficient conductivity.

2.6. Fourier transform infrared (FTIR) spectroscopy

FTIR spectra of deuterated and control CNCs of the hydrothermally treated poplar were obtained on a Spectrum Two, PerkinElmer, Waltham, MA system that was equipped with a universal attenuated-total-reflection (ATR) probe. The spectra were obtained in the range of 450–4000 cm^{-1} with a resolution of 4 cm^{-1}.

2.7. Recording Raman spectra and band intensity calculation

Cellulose, pulp, wood, and the treated wood samples were analyzed, in triplicate, with a Bruker MultiRam spectrometer (Bruker Instruments Inc., Billerica, Massachusetts). To reduce the fluorescence in the spectra the hydrothermally treated wood samples, these were analyzed after the samples had been delignified and treated with alkali (see above). The Raman system is equipped with a 1064-nm 1000 mW continuous wave (CW) diode pumped Nd:YAG laser. Sample pellets were made from ~0.1 g of each sample. The laser power used for sample excitation was 600 mW. Depending upon the S/N desired, 1024 to 2048 scans were co-added. Bruker OPUS 7.2 software was used to determine peak positions and process the spectral data. Processing of spectra involved normalization, various mathematical operations, and background removal. Background correction was performed using the "rubberband option" in OPUS using 64 baseline points. Peak heights were calculated for bands at 1096 and 93 cm^{-1} by drawing a horizontal baseline under each of the bands. For the 1096 cm^{-1} band, this was accomplished by drawing a horizontal baseline from 944 cm^{-1} (minimum intensity wavenumber near 1096 cm^{-1} peak). Similarly, for the 93 cm^{-1} peak, a horizontal baseline from 70 cm^{-1} was drawn (minimum intensity wavenumber near the peak). Additionally, for the 93 cm^{-1} band, peak areas were calculated for various samples. Using the intensity data, ratios of peak heights (93 cm^{-1} to 1096 cm^{-1}) and ratios of 93 cm^{-1} peak areas to 1096 cm^{-1} peak heights were calculated. For plotting purposes, the spectra were converted to ASCII format which then allowed the spectral data to be exported to Excel.

Sodium azide (NaN_3) was analyzed both as a solid and as aqueous solution. The solution was sampled in a shortened NMR tube and 1024 scans were co-added.

2.8. X-ray diffraction and segal-WAXS CrI calculation

Wide-angle X-ray diffraction (XRD) profiles were recorded in the reflection mode on a Bruker D8 Discover diffractometer with monochromatic CuKα (λ = 1.5418 Å) point source and a VÅNTEC-500 detector at the Materials Research Science and Engineering Center, University of Wisconsin, Madison. The X-ray diffractometer beam aperture of 0.5 mm was used. In all cases, diffractograms were obtained on the same samples (in the pellet form) that were previously analyzed by FT-Raman spectroscopy. In WAXS, both sides of the pellet were sampled and average values of the CrIs are reported. Segal-WAXS CrI was calculated by measuring intensity at plane (200), I_{200}, and subtracting the amorphous contribution, I_{am}, at approximately 2θ = 18° (Segal, Creely, Martin, & Conrad, 1959).

$$CrI = 100 \times (I_{200} - I_{am})/I_{200} \quad (1)$$

This was done after a straight line was drawn between the lowest intensity points in the 2θ range of 7° and 37°. This method is similar to the (200) peak height ratio method (Park, Baker, Himmel, Parilla, & Johnson, 2010), although in the latter method, the background subtracted was based on a blank sample run. Previously, the authors have used this approach to determine Segal CrIs (Agarwal et al., 2016, 2013; Agarwal, Ralph, Baez et al., 2017)

3. Results and discussion

3.1. Low frequency Raman spectra of cellulose materials

Fig. 1 shows low frequency (< 250 cm^{-1}) spectra from a number of cellulose materials, some of which do not contain any crystalline cellulose whereas others are highly crystalline. The former group includes amorphous cellulose (i.e., 120 min ball milled cotton MCC) and cellulose in wood that is organized but not crystalline (e.g., wood cellulose in aspen, bleached aspen, and delignified aspen). The authors have previously reported that absence of a low frequency Raman band at 93 cm^{-1} indicated that the cellulose's aggregated state was not crystalline (Agarwal et al., 2016). This observation along with many other pieces of evidence supported the hypothesis that wood cellulose in its

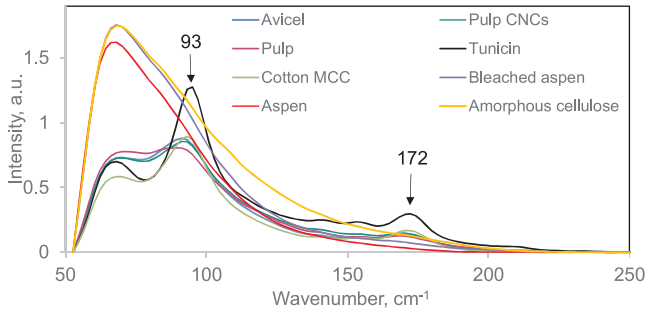

Fig. 1. Low frequency Raman spectra of various celluloses and cellulose materials.

native state is not crystalline (Agarwal et al., 2016). It was only when the wood had been either pulped or undergone a hydrothermal treatment, that the band at 93 cm^{-1} was detected (e.g., Fig. 1, spectra of pulp and pulp CNCs). On the other hand, highly crystalline cellulose I materials like tunicin and cotton MCC (Whatman CC31) showed strong contribution at 93 cm^{-1} (Fig. 1) (Agarwal et al., 2016; Agarwal, 2014).

The presence of LF bands (< 200 cm^{-1}) in Raman spectroscopy is known to be associated with a phenomenon usually linked with crystalline materials. Because the vibrational energy involved is so low, the observed bands are often lattice modes of a crystal. For example, a band at 120 cm^{-1} is detected in the crystals of NaN_3 due to the librational phonon mode (Bertsch, Rosinger, & Eysel, 1984). The band disappears when NaN_3 is dissolved in water (Fig. S1). LF contributions in crystalline cellulose are plausibly from phonon modes of the crystals and/or H-bonds (Colaianni, Aubard, Hansen, & Nielsen, 1995; Parrott et al., 2009). Indeed, based on the interaction of Terahertz (THz) radiation with optical phonons in crystal lattices, Vieira and Pasquini (Vieira and Pasquini, 2014) reported that in the case of microcrystalline cellulose a band at ~3 THz (corresponds to 99.9 cm^{-1}) was present. This is in line with the Raman bands reported at 93 cm^{-1} in Fig. 1. Therefore, to ensure that the band at 93 cm^{-1} in Raman spectra did not arise due to hydrogen-bonds, deuterated and non-deuterated (control) poplar cellulose nanocrystals (CNCs) were investigated in the low frequency region.

First, formation of the deuterated wood-CNCs was confirmed by their IR and Raman spectra (Fig. 2a and b) where, in both the techniques, bands due to O—D stretches are present in the 2500 cm^{-1} region. As expected, no such bands existed in the control poplar CNCs. More importantly, in the low frequency region of the Raman spectrum of the deuterated CNCs, shown in Fig. 2c, the band at 93 cm^{-1} did not shift or decline in intensity (spectra were normalized on the 1096 cm^{-1} band of cellulose). This result supported the contention that H-bonds did not contribute at 93 cm^{-1} and therefore, the band is likely to be due to crystalline cellulose only. The possibility that these O—D bonds, in deuterated CNCs, existed outside of the crystalline regions was negated by the fact that the bonds could not be exchanged with the OHs after various treatments in water. This indicated that such O—D groups have undergone irreversible transformation. Such treatments consisted of the following actions on the hydrothermally treated samples, in D_2O at 200 °C, that was subsequently delignified – (a) oven drying at 110 °C in H_2O and (b) heating in water at 90 °C for 4 h at pHs 3, 5, 8.5, and 12. The Raman spectra of the variously-treated and control wood samples are shown in Fig. S2. In Fig. S2, the Raman spectrum of the delignified sample that was sampled in H_2O showed that the OD groups were retained in presence of water. These results are in agreement with the finding from another investigation where the OH to OD transformation was reported to be irreversible (Ponni, Kontturi, & Vuorinen, 2013).

3.2. Amorphous nature of 120 min ball-milled cellulose

To ensure that the 120 min ball-milled Whatman CC31 sample was completely amorphous, the control and ball-milled samples were analyzed by scanning electron microscopy (SEM), Raman spectroscopy, and XRD. Upon ball-milling, the SEMs indicated complete morphological change in the control sample from a fiber like appearance (Fig. 3a) to spherical particles much reduced in size (Fig. 3b). There was no residual fiber like material left after 120 min of ball-milling. For these samples, Raman spectra are shown in Fig. 3c and it can be noted that the spectra support complete de-crystallization due to total disappearance of the 380 cm^{-1} band of cellulose (Agarwal et al., 2010). Moreover, as expected, a new band due to amorphous cellulose appeared at 357 cm^{-1} (Agarwal et al., 2010). A similar behavior was displayed by the band at 93 cm^{-1} which, in the ball-milled sample, lost its intensity completely (Fig. 3c). However, no new band due to the amorphous phase of cellulose appeared in the LF region. The two samples were also analyzed by XRD and the diffractograms are shown in Fig. 3d. Once again the diffractograms indicated complete de-crystallization of the cotton MCC sample (Agarwal et al., 2016).

3.3. 93 cm^{-1} band based method

To find out if another cellulose CrI estimation method can be developed based on the 93 cm^{-1} Raman band of cellulose, six calibration set samples were prepared by mixing high CrI cotton microcrystalline cellulose (Whatman CC31) and 120-min ball-milled completely amorphous cellulose in various proportions (Table 1). This approach is identical to what has been done previously by the authors and other researchers (Agarwal et al., 2010; Schenzel, Fischer, & Brendler, 2005). The CrI of each of the calibration set samples can be defined by the crystalline fraction, X_c, present (Eq. (2)).

$$X_c = M_c/M_t = M_c = M_c/(M_c + M_a) \quad (2)$$

Where M_c, M_a, and M_t are the crystalline, amorphous, and total mass fractions of cellulose, respectively. Since $M_c = X_{control} \times M_{control}$, where $X_{control}$ and $M_{control}$ are the % CrI and mass fraction of the control sample (80.5% CrI based on Segal-WAXS, Table 1). The above equation can be re-written as

$$X_c = X_{control} \times M_{control}/(M_c + M_a) = 80.5 \times M_{control}/(M_c + M_a) \quad (3)$$

The crystallinities of six of the eight calibration set samples were calculated using Eq. (3) (calculated crystallinities, Table 1; as in Agarwal et al., 2010) and these values were based on WAXS data for control and 120-min milled samples. The Segal-WAXS CrI data was taken from a prior publication (Agarwal et al., 2010). In addition to 93-Raman based CrIs (see below), Table 1 lists previously reported CrIs that were obtained using Segal-WAXS and 380-Raman methods. In the 93-Raman method, because no contribution at 93 cm^{-1} band was seen from the amorphous cellulose (Fig. 3c), the entire contribution was taken as the crystalline portion of the samples. The Raman spectra of the calibration set samples (six mixtures, amorphous cellulose, and control Whatman CC31; Table 1) were obtained. Following that, the intensity (both peak height and area) ratios of the 93 cm^{-1} band to 1096 cm^{-1} band (only peak height) for various samples were calculated. The 1096 cm^{-1} band intensity served as an internal reference and compensated for any changes in Raman experiment variables (e.g., pellet density variations, laser power changes during the scans, and scattering geometry changes). Fig. 4a contains the background corrected and 1096 cm^{-1} normalized spectra of the eight samples.

Next, the band intensity ratios were plotted against the calculated calibration set crystallinities (Table 1). The Raman ratio plots for I_{93}/I_{1096} (Fig. 4b) generated excellent regressions (R^2 = 0.9888 and 0.9884 for peak height (PH) and peak area, respectively) and showed good sensitivity to CrI change.

Although both regressions were equally good, the pH regression is preferred due to the prospect that in certain samples a neighboring band may appear and partially overlap with the profile of the 93 cm^{-1} band. In that scenario, between the band area and PH CrI

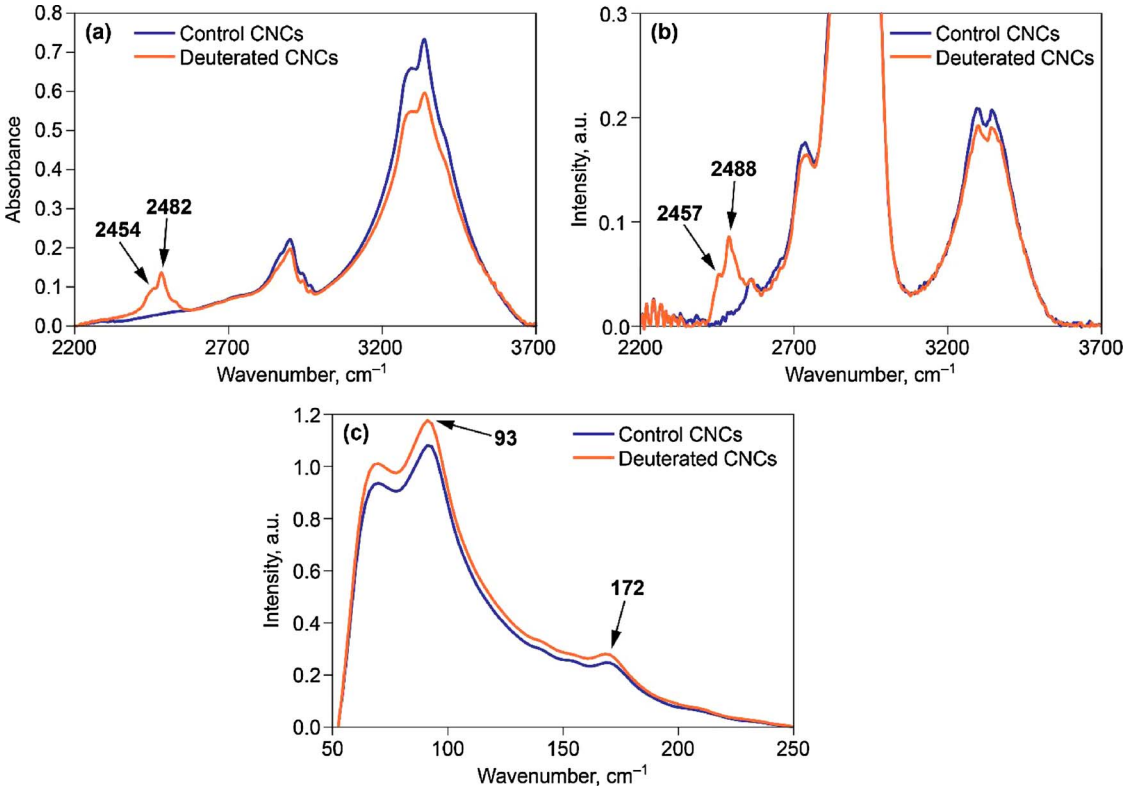

Fig. 2. Spectra of control and deuterated poplar CNCs. (a) IR spectra in 2200–3700 cm^{-1} region, (b) Raman spectra in 2200–3700 cm^{-1} region, (c) Raman spectra of CNCs in 50–250 cm^{-1} region.

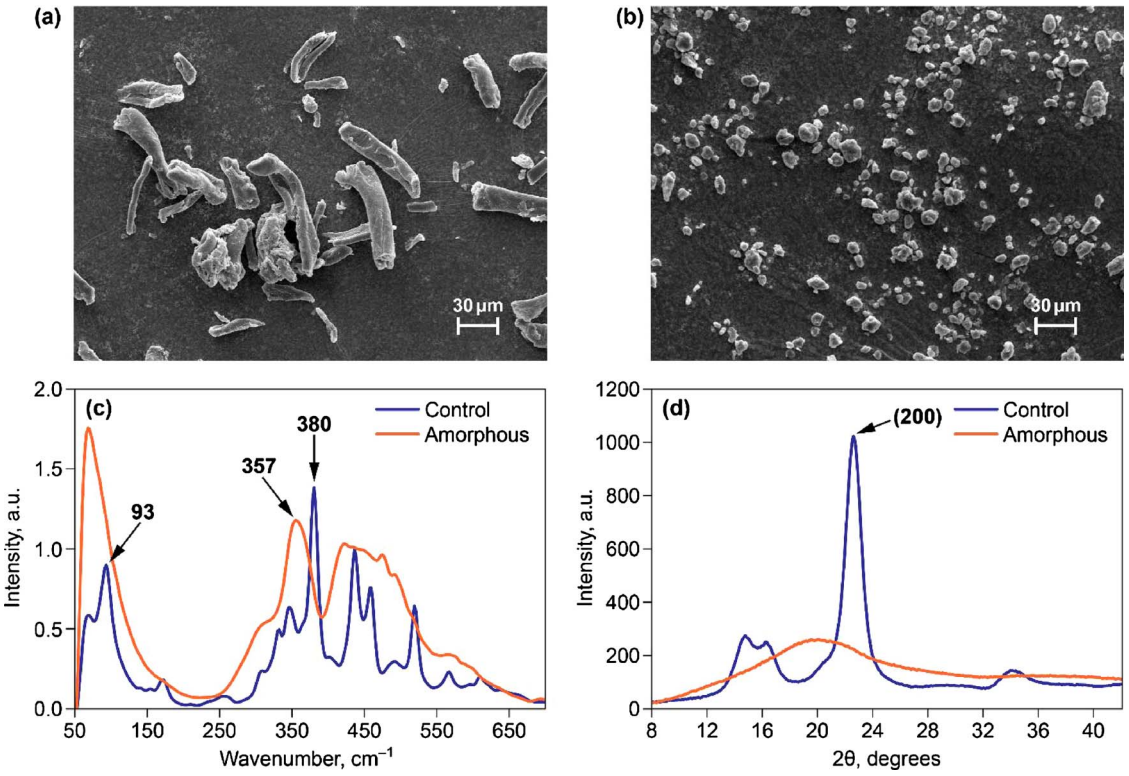

Fig. 3. (a) SEM of control Whatman CC31, (b) SEM of 120 min ball-milled Whatman CC31, (c) Raman spectra of control and 120 min ball-milled Whatman CC31, (d) XRDs of control and 120 min ball-milled Whatman CC31.

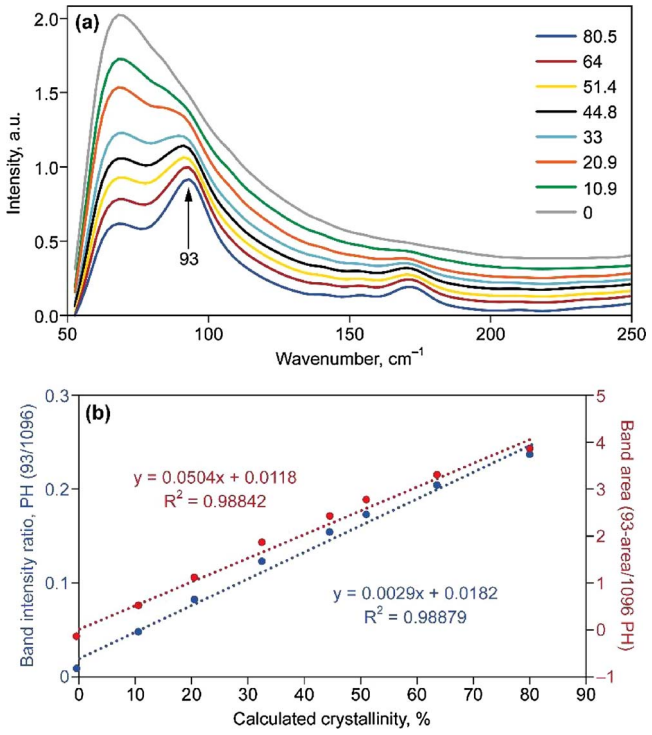

Fig. 4. (a) Low frequency Raman spectra of calibration set samples, calculated CrIs of the samples are listed in (a); (b) Correlations of the calibration set crystallinities, 93-peak height and 93-peak area ratios, against calculated crystallinities.

measurements, the former is more likely to be impacted. Therefore, considering the excellent fit between the calculated crystallinities and the 93 cm^{-1} PH intensity ratios (Fig. 4b), the correlation obtained should be used to estimate crystallinities in cellulose I containing materials. The correlation equation is,

$$X_{93\text{-}Raman} = ((I_{93}/I_{1096}) - 0.0182)/0.0029 \quad (4)$$

Repeat Raman measurements of the calibration set samples produced an average standard error of ± 0.86% (Table 1 for individual SD data) and indicated that the 93-Raman CrI model was reliable. The error was calculated from three replicate Raman acquisitions at different locations of the pellet of each of the eight calibration set samples.

The same calibration set samples have been previously analyzed using 380-Raman methods and Segal-WAXS and the data are shown in Table 1 (Agarwal et al., 2010). The 93-Raman CrI data (Table 1) showed excellent correlation with this data (Fig. 5a). The regression coefficients for the 380-Raman and WAXS-Segal versus 93-Raman were 0.9968 and 0.9713, respectively (Fig. 5). This indicated that, for the calibration set samples, 93-Raman method correlated very well with the other two methods.

Although for the calibration samples the 93-Raman method was highly correlated to the other two methods, in general, cellulose aggregates in more complex supramolecular states (e.g., non-crystalline, disordered, ordered, and organized) than what existed in the mixture pellets (crystalline, amorphous or a combination of these two phases). The latter states are rarely encountered in practice and it is the former aggregated states for which the 93- method does a superior job (more below).

3.4. CrI estimation using 93-Raman method

The 93-Raman method was used to determine crystallinities of a number of cellulose materials (Table 2). For the samples listed in Table 2, CrIs were also determined by 380-Raman and Segal-WAXS methods. In case of amorphous cellulose, Segal-WAXS CrI of 23.2%

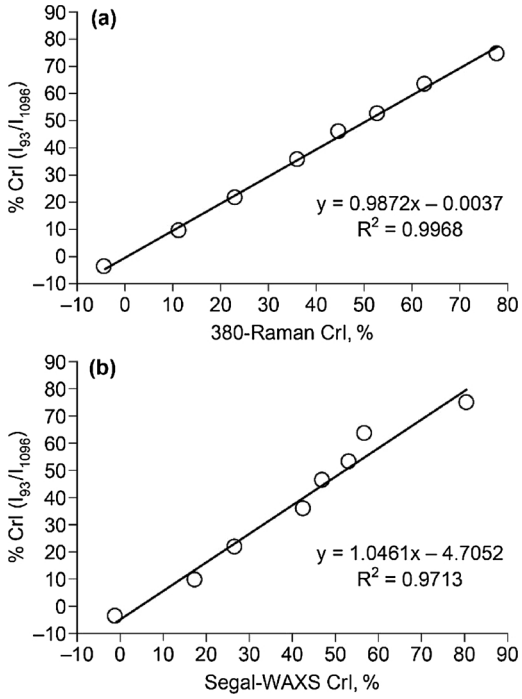

Fig. 5. Correlations of the calibration set crystallinities, (a) 93-peak height against 380-Raman and (b) 93-peak height against Segal-WAXS; Table 1 data.

Table 2
Percent Crystallinities of cellulose materials – 93-Raman, 380-Raman, and Segal-WAXS.

Samples	93-Raman	Normalized 93-Raman	380-Raman	Segal-WAXS
Tunicin	120.1	100.0	86.5[a]	97.2
Cotton MCC	74.7	62.2	82.2[a]	93.5[a]
Avicel	49.9	41.5	59.1[a]	87.5[a]
Bleached kraft pulp[b]	36.7	30.6	53.2[a]	82.5[a]
Pulp CNCs[c]	40.4	33.6	55.5	84.4
Aspen wood	0 0.0	0.0	49.9[a]	77.0[a]
200 °C heated poplar wood	41.3	34.4	65.0	81.3
Poplar CNCs[d]	55.9	46.5	62.0	91.5
Amorphous cellulose	−3.5	−2.9	−4.4[e]	23.2[a]

[a] Agarwal et al. (2016).
[b] Softwood.
[c] From softwood bleached kraft pulp.
[d] From 200 °C heated poplar.
[e] Agarwal et al. (2010).

(Table 2) is reported. This differs from the value (−1%) reported in Table 1 for this sample. This is due to the fact that two different approaches were used to evaluate the XRD scattering curves. In Table 1, a modified method (Agarwal et al., 2010) was used where instead of measuring (and subtracting) amorphous contribution at 18°, the contribution was measured at 21° (because XRD of amorphous cellulose has a peak at 21°). When the amorphous contribution is measured at 18° (Agarwal et al., 2016), a much higher value of crystallinity (23.2%, Table 2) was obtained. In the 93-Raman method, the CrI of tunicin which is totally crystalline (Agarwal et al., 2016) was estimated to be 120% (Table 2). This value is above 100% due the fact that the 93-Raman CrIs are based on the correlation (Eq. (4)) which depends upon calculated crystallinities (Fig. 4b) that, in turn, are based on the Segal-WAXS values (Table 1). It is well recognized that the latter method overestimates true crystallinities (Park et al., 2010). Therefore, to keep the 93-Raman values for all samples at 100% or lower, the CrIs were normalized to tunicin CrI (93-Raman normalized, Table 2). By doing this, tunicin had the highest CrI value possible of 100%. The estimated

CrIs from the three methods (Table 2) are plotted in Fig. S3. Although by the three methods tunicin was found to be the most crystalline, important differences existed between the CrIs of various samples (Fig. S3). Except for the CrI of tunicin, where the Segal-WAXS value was slightly lower than the 93-Raman estimation (normalized data), in all other cases, CrIs by the Segal-WAXS were the highest (Table 2). For these seven samples, excluding tunicin and amorphous cellulose, the order of the methods for high to low absolute values of the CrIs was Segal-WAXS > 380-Raman > 93-Raman. Moreover, irrespective of the fact that the absolute CrIs were different between the methods, the CrI-order of the samples (e.g., from high to low) was different between any two methods (Table 2). This is likely to be due to not only the differences that are inherent to the methods but also, the sample characteristics that influence the methods differently. For instance, lignin as a sample component impacts 380-Raman and Segal-WAXS differently (Agarwal et al., 2013). Even more importantly, the state of aggregation of cellulose itself has an influence.

Unfortunately, in literature, the latter issue has not been carefully investigated. An important result of the authors' studies was that, unlike other methods, the 93-Raman CrI of aspen wood was zero. The result has been previously reported and used to support the finding that wood cellulose in the native state in not crystalline (Agarwal et al., 2016). The zero CrI of wood cellulose by 93-Raman method is not unique to aspen woods; other woods were also found to be non-crystalline (authors' unpublished results). For the aspen wood sample, the CrIs by the other methods were non-zero and significantly higher (e.g., 49.9 and 77.0% by 380-Raman and Segal-WAXS, respectively, Table 2). The reason for this discrepancy has to do with the inability of the other methods (380-Raman, Segal-WAXS, and NMR) to distinguish between organized and crystalline celluloses. As reported earlier (Agarwal et al., 2016; Li and Renneckar, 2011; Li et al., 2017; Su et al., 2015), in these methods, this ensues due to the contributions of crystalline and "non-crystalline but organized" celluloses being present in the same spectral/diffraction regions.

3.5. Hydrothermal treatment of poplar wood

It is known that hydrothermally treated woods are more durable and provide resistance to bio decay (Assor et al., 2009; Inagaki, Siesler, Mitsui, & Tsuchikawa, 2010; Sundqvist, Karlsson, & Westermark, 2006; Yin, Berglund, & Salmen, 2011). Moreover, it has been reported that upon such treatments cellulose CrI is increased (Inagaki et al., 2010). The increased resistance to decay of the hydrothermally treated wood is due to the wood becoming less hydrophilic. Recently, the authors have used the hydrothermal treatment to produce CNCs from wood (Agarwal et al., 2016; Agarwal, Ralph, Reiner, & Baez, 2017). Production of CNCs directly from wood became possible due to cellulose becoming partly crystalline upon hydrothermal treatment (Inagaki et al., 2010). Therefore, to study this transformation of cellulose to a partly crystalline state, the 93-Raman method was applied to study hydrothermally treated poplar wood samples that were treated at different temperatures. The LF Raman spectra of such samples and corresponding CrI data are shown in Fig. 6a. The spectra were obtained after the samples were mostly delignified and treated in 4% NaOH. These treatments were necessary to remove most of the sample fluorescence which can otherwise be a problem in Raman spectroscopy. Almost complete sample delignification was necessary to avoid the lignin-caused fluorescence in the hydrothermally treated samples. The alkali treatment removed the residual lignin along with some of the hemicelluloses. In this context, it is important to note that it has been shown that the delignification treatment causes no significant change in a sample's CrI (Agarwal, Ralph, Reiner, Moore, & Baez, 2014).

When Fig. 6a CrI data were plotted against the temperatures of the hydrothermal treatment a linear relationship (R^2 = 0.9234) was obtained (Fig. 6b) suggesting that higher the treatment temperature higher the CrI. This is useful information because using temperature as a variable, wood materials with varying CrIs and desirable properties can be generated. Such materials would have many applications depending upon their specific properties and needs of the applications.

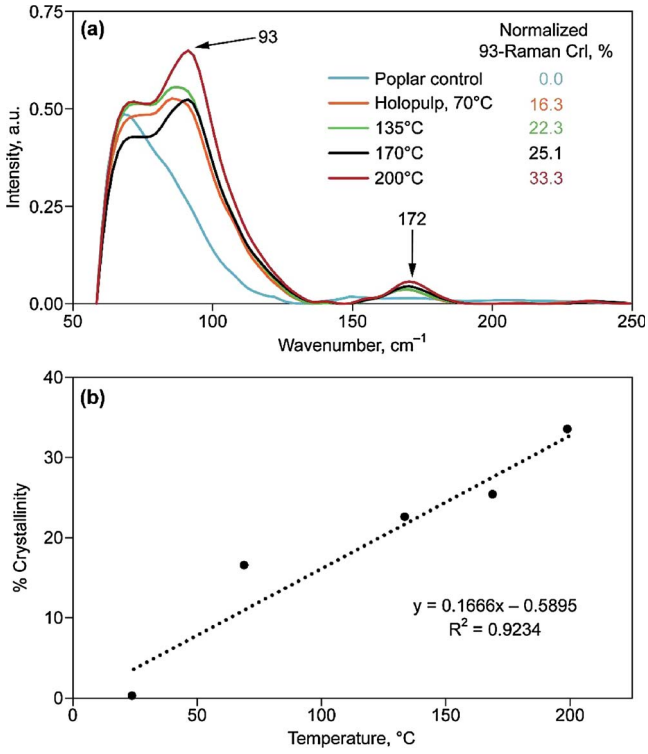

Fig. 6. (a) Low frequency Raman spectra of control and hydrothermally treated poplar wood; (b) 93-Raman crystallinity as a function of temperature of hydrothermal treatment of poplar wood.

In Fig. 7, based on previously proposed model (Fig. 7a) of native wood cellulose ultrastructure (Agarwal et al., 2016), a scheme is proposed that illustrates how the non-crystalline wood cellulose is converted to partly crystalline form upon hydrothermal treatment (Fig. 7b). On one hand, in the native state, only disordered and consolidated regions exist in cellulose (Fig. 7a) (Agarwal et al., 2016), but upon hydrothermal treatment, these regions are partly converted into crystalline and coalesced segments in cellulose (Fig. 7b). Both the regions are expected to be modified upon hydrothermal treatment at 200 °C although the extent of D_2O accessibility of the consolidated region is likely to be limited. The transformation can be understood in terms of role of water in cellulose aggregation under different thermodynamic conditions (Silveira, Stoyanov, Kovalenko, & Skaf, 2016). Silveira et al. (2016) showed that under ambient conditions, highly structured hydration shells around cellulose create repulsive forces that protect cellulose microfibrils from aggregating. Under hydrothermal pretreatment conditions, however, the hydration shells lose structure, and cellulose aggregation is favored. In the context of present work, same phenomenology would apply but at the cellulose molecular level where the hydration shells exist around cellulose molecules and upon hydrothermal pretreatment, they lose structure and cellulose crystallization or coalescence occurs.

3.6. Organized vs. crystalline phases

It has been reported that wood cellulose in the native state is not crystalline (Agarwal et al., 2016). This is reinforced by the LF Raman spectra of various aspen wood samples (Fig. 1) and the CrI data of aspen wood in Table 1. In Fig. 1, no peak at 93 cm^{-1} was detected implying absence of crystalline cellulose in aspen, alkaline H_2O_2 bleached aspen, and delignified aspen wood samples (Agarwal et al., 2013). On the

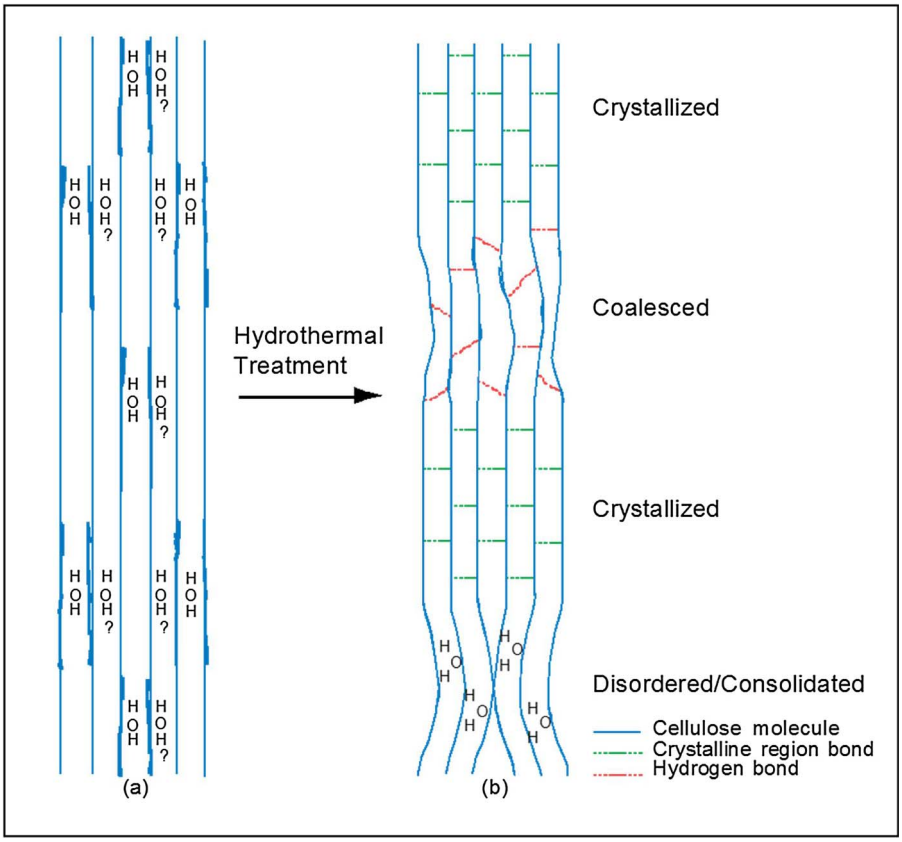

Fig. 7. Proposed hydrothermal treatment caused transformation of non-crystalline native wood cellulose (a) (Agarwal et al., 2016) to partly crystalline cellulose (b). The ? means that it is unknown if such a location is accessible by water.

other hand, these samples contributed at 380 cm^{-1} and ~22.3° 2θ, respectively, in Raman spectroscopy and XRD (Fig. 8) (Agarwal et al., 2013). In Fig. 8a, Raman spectra are plotted after they were normalized at 1096 cm^{-1} band of cellulose. Therefore, the CrIs estimated from the 380-Raman and Segal-WAXS methods were non-zero and significant (Agarwal et al., 2013). For example, the 380-Raman and Segal-WAXS CrIs for the aspen wood are 49.9 and 77%, respectively (Table 2). The only explanation for the contradictory CrI information that native wood cellulose is crystalline by Segal-WAXS and 380-Raman and non-crystalline by 93-Raman is that the contributions seen at 380 cm^{-1} in Raman spectrum and ~22.3° 2θ in XRD are due to spatially organized cellulose. Such cellulose is not crystalline although crystalline cellulose when present also makes contributions in these regions. This explanation is supported by the information mentioned earlier that, in Raman spectroscopy, XRD, and NMR, the molecularly thick non-crystalline ultrathin microfibril fractions contributed in the same regions where contributions of crystalline domains are detected (Agarwal et al., 2016; Li and Renneckar, 2011; Li et al., 2017; Su et al., 2015). Therefore, the new 93-Raman method is capable of differentiating between organized and crystalline phases of cellulose.

4. Conclusions

A new cellulose CrI estimation method based on the 93 cm^{-1} Raman band of cellulose was developed. The 93-Raman method based crystallinities of calibration set samples correlated well with those estimated using 380-Raman and Segal-WAXS methods. The method performed well when applied to select cellulose materials with varying crystallinities. A unique aspect of the 93-Raman method is that the determined CrI is not influenced by the presence of organized non-

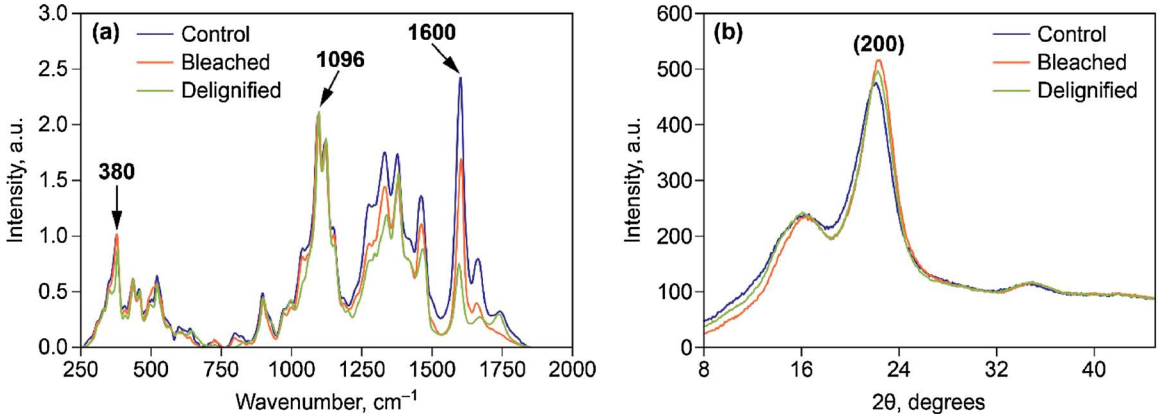

Fig. 8. (a) Raman spectra of control, H_2O_2 bleached, and delignified aspen; (b) XRDs of control, H_2O_2 bleached and delignified aspen.

crystalline cellulose and therefore, the method has an advantage in situations where the latter condition exists. To study the development of CrI in wood cellulose, the method was applied to investigate poplar wood samples that were hydrothermally treated at different temperatures. It was found that more crystalline cellulose was formed at higher treatment temperatures.

Author contributions

The manuscript was written through contributions of all authors. All authors have given approval to the final version of the manuscript.

Acknowledgements

The authors thank Dr. Johan Foster (Virginia Polytechnic Institute and State University) for providing Tunicates. Also, Tom Kuster (retired) of Analytical Chemistry and Microscopy Laboratory is acknowledged for his help in obtaining SEMs. The authors gratefully acknowledge use of X-ray facilities and instrumentation supported by NSF through the University of Wisconsin Materials Research Science and Engineering Center (DMR-1121288).

Appendix A. Supplementary data

Supplementary data associated with this article can be found, in the online version, at https://doi.org/10.1016/j.carbpol.2018.03.003.

References

Agarwal, U. P., Reiner, R. S., & Ralph, S. A. (2010). Cellulose I. Crystallinity determination using FT–Raman spectroscopy: Univariate and multivariate methods. *Cellulose, 17*, 721–733.

Agarwal, U. P., Reiner, R. S., & Ralph, S. A. (2013). Estimation of cellulose crystallinity of lignocelluloses using near-IR FT–Raman spectroscopy and comparison of the Raman and Segal-WAXS methods. *Journal of Agricultural and Food Chemistry, 61*, 103–113.

Agarwal, U. P., Ralph, S. A., Reiner, R. S., Moore, R. K., & Baez, C. (2014). Impacts of fiber orientation and milling on observed crystallinity in jack pine. *Wood Science and Technology, 48*, 1213–1227.

Agarwal, U. P., Ralph, S. A., Reiner, R. S., & Baez, C. (2016). Probing crystallinity of never-dried wood cellulose with Raman spectroscopy. *Cellulose, 23*, 125–144.

Agarwal, U. P. (2014). 1064 nm FT-Raman spectroscopy for investigations of plant cell walls and other biomass materials. *Frontiers in Plant Science, 5*, 490.

Agarwal, U. P., Ralph, S. A., Baez, C., Reiner, R. S., & Verrill, S. P. (2017). Effect of sample moisture content on XRD-estimated cellulose crystallinity index and crystallite size. *Cellulose, 24*, 1924–1971.

Agarwal, U.P., Ralph, S.A., Reiner, R.S., Baez, C., (2017). Production of cellulose nanocrystals from raw wood via hydrothermal treatment. US Patent Application 20170260692, http://www.freepatentsonline.com/y2017/0260692.html. (Accessed 1 November, 2017).

Ahlgren, P. A., & Goring, D. A. I. (1971). Removal of wood components during chlorite delignification of black spruce. *Canadian Journal of Chemistry, 49*, 1272–1275.

Assor, C., Placet, V., Chabbert, B., Habrant, A., Lapierre, C., Pollet, B., et al. (2009). Concomitant changes in viscoelastic properties and amorphous polymers during the hydrothermal treatment of hardwood and softwood. *Journal of Agricultural and Food Chemistry, 57*, 6830–6837.

Bertsch, G., Rosinger, G., & Eysel, H. H. (1984). Raman intensities and electro-optical parameters of the azide ion in P-NaN3 single crystals and aqueous solution. *Journal of Raman Specroscopy, 15*, 414–420.

Bower, D. I., & Maddams, W. F. (1989). *The vibrational spectroscopy of polymers.* Cambridge, UK: Cambridge University Press227–306.

Colaianni, S. E. M., Aubard, J., Hansen, S. H., & Nielsen, O. F. (1995). Raman spectroscopic studies of some biochemically relevant molecules. *Vibrational Spectroscopy, 9*, 111–120.

Inagaki, T., Siesler, H. W., Mitsui, K., & Tsuchikawa, S. (2010). Difference of the crystal structure of cellulose in wood after hydrothermal and aging degradation: A NIR spectroscopy and XRD study. *Biomacromolecules, 11*, 2300–2305.

Li, Q., & Renneckar, S. (2011). Supramolecular structure characterization of molecularly thin cellulose I nanoparticles. *Biomacromolecules, 12*, 650–659.

Li, Z., Sathitsuksanoh, N., Zhang, W., Goodell, B., & Renneckar, S. (2017). In U. P. Agarwal, R. H. Atalla, & A. Isogai (Eds.). *The nano-structures of native celluloses, their transformations upon isolation, and their implications for production of nanocelluloses*Washington DC: American Chemical Society ACS Symposium Series #1251, Chapter 3.

Paolantoni, M., Sassi, P., Morresi, A., & Santini, S. (2007). Hydrogen bond dynamics and water structure in glucose-water solutions by depolarized Rayleigh scattering and low-frequency Raman spectroscopy. *The Journal of Chemical Physics, 127*, 024504.

Park, S., Baker, J. O., Himmel, M. E., Parilla, P. A., & Johnson, D. K. (2010). Cellulose crystallinity index: measurement techniques and their impact on interpreting cellulase performance. *Biotechnology for Biofuels, 3*, 10.

Parrott, E. P. J., & Zeitler, J. A. (2015). Terahertz time-domain and low-frequency Raman spectroscopy of organic materials. *Applied Spectroscopy, 69*, 1–25.

Parrott, E. P. J., Zeitler, J. A., Friščić, T., Pepper, M., Jones, W., Day, G. M., et al. (2009). Testing the sensitivity of terahertz spectroscopy to changes in molecular and supramolecular structure: A study of structurally similar cocrystals. *Crystal Growth and Design, 9*, 1452–1460.

Ponni, R., Kontturi, E., & Vuorinen, T. (2013). Accessibility of cellulose: Structural changes and their reversibility in aqueous media. *Carbohydrate Polymers, 93*, 424–429.

Reiner, R. S., & Rudie, A. W. (2013). In M. T. Postek, R. J. Moon, A. J. Rudie, & M. A. Bilodeau (Eds.). *Production and applications of cellulose material* (pp. 21–24). Atlanta: TAPPI Press.

Schenzel, K., Fischer, S., & Brendler, E. (2005). New method for determining the degree of cellulose I CrI by means of FT Raman spectroscopy. *Cellulose, 12*, 223–231.

Segal, L., Creely, J. J., Martin, A. E., & Conrad, C. M. (1959). An empirical method for estimating the degree of crystallinity of native cellulose using the x-ray diffractometer. *Textile Research Journal, J29*, 786–794.

Silveira, R. L., Stoyanov, S. R., Kovalenko, A., & Skaf, M. S. (2016). Cellulose aggregation under hydrothermal pretreatment conditions. *Biomacromolecules, 17*, 2582–2590.

Su, Y., Burger, C., Ma, H., Chu, B., & Hsiao, B. S. (2015). Exploring the nature of cellulose microfibrils. *Biomacromolecules, 16*, 1201–1209.

Sundqvist, B., Karlsson, O., & Westermark, U. (2006). Determination of formic-acid and acetic acid concentrations formed during hydrothermal treatment of birch wood and its relation to color, strength, and hardness. *Wood Science and Technology, 40*, 549–561.

Vieira, F. S., & Pasquini, C. (2014). Determination of cellulose crystallinity by terahertz-time domain spectroscopy. *Analytical Chemistry, 86*, 3780–3786.

Yin, Y., Berglund, L., & Salmen, L. (2011). Effect of steam treatment on the properties of wood cell walls. *Biomacromolecules, 12*, 194–202.